Analysis and Design of a Delta-Type Interior Permanent Magnet Synchronous Generator by Using an Analytic Method

DONG-KUK LIM [1], (Member, IEEE), AND JONG-SUK RO [2]
[1] School of Electrical Engineering, University of Ulsan, Ulsan 44610, South Korea
[2] School of Electrical and Electronics Engineering, Chung-Ang University, Seoul 06974, South Korea

Corresponding author: Jong-Suk Ro (jongsukro@gmail.com)

ABSTRACT The analytic analysis of delta-type interior permanent synchronous machines is difficult due to the absence of a useful analytic method, especially considering the high magnetic saturation effect of the machine. Hence, the nonlinear magnetic equivalent circuit (MEC) method, which considers the severe magnetic saturation of the iron core, is proposed in this paper. With the proposed nonlinear MEC method, the characteristics of the delta-type interior permanent magnet synchronous generator (IPMSG) are precisely calculated and the computational burden is remarkably reduced. The proposed MEC method is validated by comparing the calculated data with the experimental results.

INDEX TERMS Finite element method (FEM), interior permanent magnet synchronous generator (IPMSG), magnetic equivalent circuit (MEC), range extended electric vehicle (REEV).

I. INTRODUCTION

Large electric vehicles (EVs) have some prominent issues, such as a long charging time, large battery weight, and a lack of charging stations. Hence, range extended electric vehicles (REEVs) have gained attention as a realistic solution, since they can increase one time charging mileage by using a generation system that charges batteries during a drive [1], [2].

The important requirements in the generator design for the REEV are the maximization of power density to improve the mileage and to generate enough power and the minimization of torque ripple to improve the output power quality, controllability, and riding impression. To satisfy these requirements, the interior permanent magnet (IPM) machine was chosen as the ideal generator type for the REEV. Since IPM machines have high power density and high efficiency characteristics, they are extensively used in various applications such as EVs, washing machines, and drones [3]–[5]. Furthermore, the

The associate editor coordinating the review of this manuscript and approving it for publication was Xue Zhou.

delta-type rotor construction is applied in order to reduce the torque ripple through the reduction of the total harmonic distortion (THD) of the back-electromotive force (EMF).

With respect to machine analysis, it is difficult to analyze the IPM synchronous generator (IPMSG) using an analytical method such as a magnetic equivalent circuit (MEC) due to the complicated structure and magnetic saturation of the iron core. Especially, the delta-type rotor construction causes a high magnetic saturation effect. Hence, the finite element method (FEM) is most often applied to the analysis and design of IPM machines. Although the FEM can accurately calculate the IPM machine characteristics, it requires excessive time and effort during the analysis and design of IPM machines [6], [7], [9].

To deal with this problem, we propose a nonlinear MEC method that can consider the complex structure and high magnetic saturation by use of segmented adjustable reluctances and iterative calculations with an actual *BH* curve. Since the back-EMF and the THD of the back-EMF can be computed accurately by using the proposed nonlinear MEC, it is a very effective analysis method for the early design stage

of the delta-type IPMSG. In addition, the feasibility of the proposed MEC is verified through comparison with the FEM and experimental results and design of the delta-type IPMSG for the REEV.

II. DELTA-TYPE ROTOR CONSTRUCTION OF IPMSG

In terms of power density and torque ripple, the delta-type IPMSG, as illustrated in Fig. 1, shows an outstanding over-all performance. The IPM machine has the advantages of high reluctance torque caused by saliency compared with the surface-mounted permanent magnet machine [8]. In addition, the multi-layered permanent magnet construction of the delta-type IPMSG generates more reluctance torque than the single-layered one [8], [9].
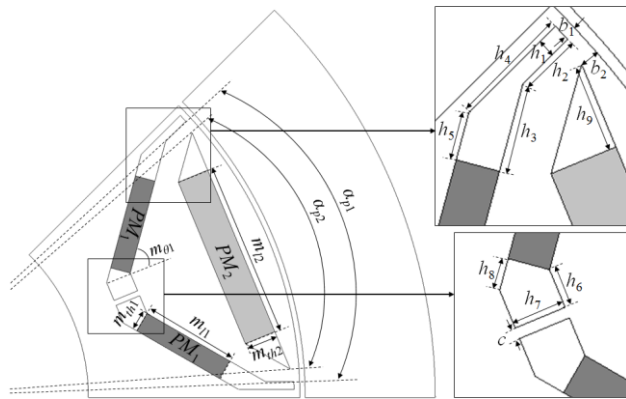
**FIGURE 1.** Delta-type rotor configuration and design variables.

Furthermore, the THD of the back-EMF can be alleviated by regulating the saturation level, which is determined through the strength and shape of the magnet placed on the outside of the rotor. In other words, the THD of back-EMF and torque ripple can be reduced by an intentional saturation design of the outside of the rotor in the delta-type IPMSG [2].

From the viewpoint of analysis, it is difficult to analyze the delta-type IPMSG by using an analytical method such as MEC due to the high saturation effect. Hence, FEMs are typically applied to the design of the delta-type IPMSG. However, when the FEM is used in the early stage of the motor design process, too much computational time is required [6], [7, [9].

III. NONLINEAR MEC METHOD

To deal with the problem of computational time associated with the FEM, the nonlinear MEC method is proposed in this paper. Most importantly, the initial design results can be rapidly derived by using the proposed MEC method in the early design stage [9].

Fig. 2 shows the flux lines of the delta-type IPMSG (ϕ_r: the flux sources over one magnet pole, ϕ_g: the flux passing through air-gap, ϕ_{mb}: the leakage flux of PM over one magnet pole, ϕ_{ml}: the magnet end-leakage flux, and ϕ_{mb} and ϕ_{mc}: the leakage flux through the bridge and the center post, respectively).
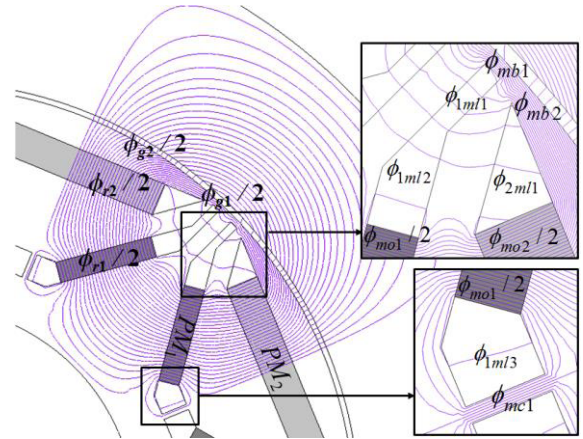
FIGURE 2. Flux density and segmented modeling of the saturation region.
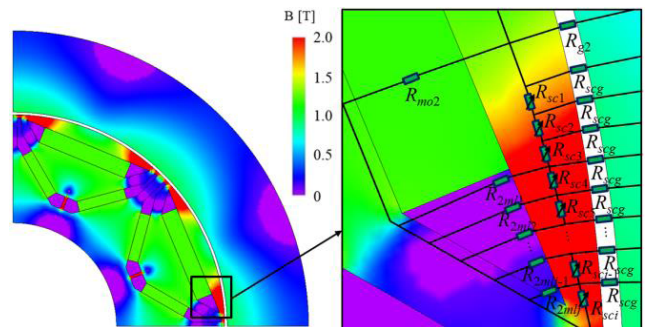
FIGURE 3. Flux density and segmented modeling of the saturation region.

The left figure of Fig. 3 represents the flux density distribution of the delta-type IPMSG. There are very severe saturation regions on both sides of the magnet on the outside of the rotor to reduce the THD of the back-EMF [2]. The right figure of Fig. 3 shows the segmented modeling of the saturation region which is bridge of the rotor. Although the bridges cause the flux leakage, they are necessary for mechanical stability. Since the bridges are made by strong iron, the scattering of the magnet due to the centrifugal force can be prevented [9]. They are designed to be highly saturated in order to guarantee the mechanical strength and minimize the flux leakage. Furthermore, this highly saturated bridge makes the sinusoidal air-gap flux density and back-EMF. In other words, the THD of back-EMF and torque ripple can be reduced by an intentional saturation design of the bridge.

In Fig. 4, the nonlinear MEC is constructed based on the flux paths explained in Fig. 2 and Fig. 3. The red box in the Fig. 4 represents the segmented modeling of the saturation region as shown in the right figure of Fig. 3.

The reluctances of the unsaturated stator and rotor iron core can be ignored, since these parts have considerably high permeability compared with those of the air-gap or saturated region in the rotor [7]. Ignoring the reluctance of the stator and rotor, Fig. 4 is converted to Fig. 5 to simplify the calculations using symmetry [9].

For an accurate analysis of the saturation region, nonlinear iterative analysis of the adjustable reluctance, R_{rc} is applied.
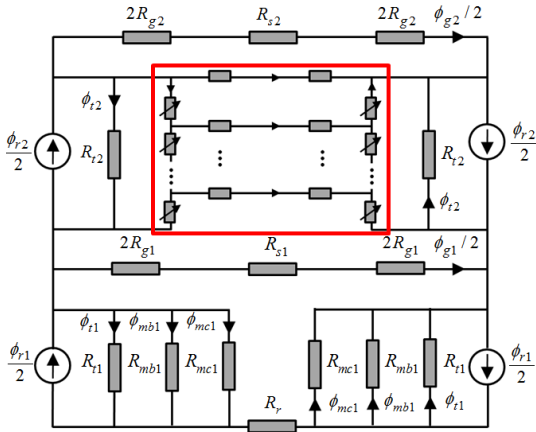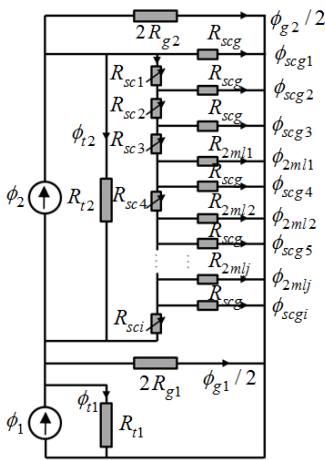
FIGURE 4. Nonlinear MEC of delta-type IPMSG.

FIGURE 5. Simplified nonlinear MEC of delta-type IPMSG.

The fluxes of the first and the second layer, ϕ_1 and ϕ_2, as shown in Fig. 5, are computed by using (1) and (2):

$$\phi_1 = \frac{\phi_{r1}}{2} - \phi_{mb1} - \phi_{mc} \qquad (1)$$

$$\phi_2 = \frac{\phi_{r2}}{2}. \qquad (2)$$

The reluctance of the first and the second layer, R_{t1} and R_{t2}, respectively, are calculated as follows:

$$R_{t1} = 2R_{mo1} // R_{1ml1} // R_{1ml2} // R_{1ml3} \qquad (3)$$
$$R_{t2} = 2R_{mo2} // R_{2ml1} \qquad (4)$$

where R_{mo} is the leakage reluctance of the magnet and R_{ml} is the magnet end-leakage reluctance. The basic process of the MEC modeling is the same as the method of the preceding research, discussed in reference [7], [9].

Fig. 6 shows the flow chart for the nonlinear MEC for the iterative calculation of the saturation effect. To calculate the saturation, a segmented number of i fluxes of the saturated core are repeatedly computed k times. If the permeabilities of the segmented core are determined in the kth iteration, the kth nonlinear MEC can be calculated. In the first iteration, users decide the permeabilities of all the segments. Then, the
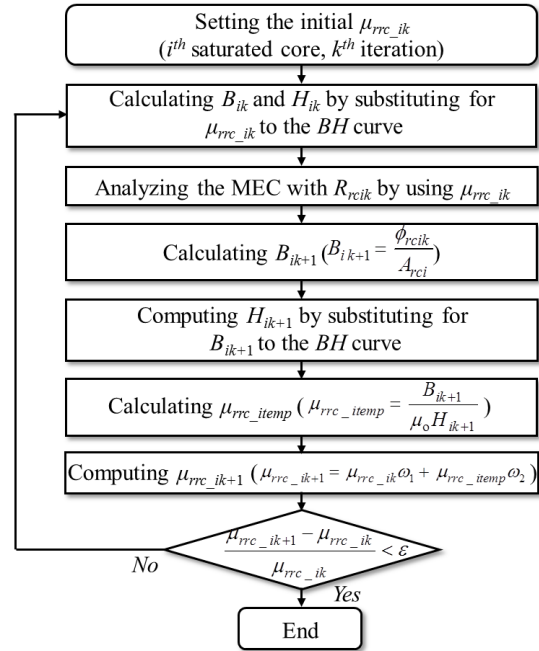

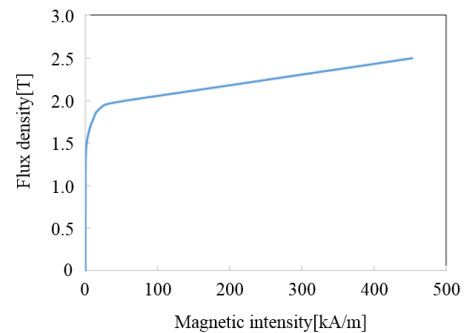**FIGURE 6. Flow chart for the nonlinear MEC calculation.**

FIGURE 7. Actual BH curve of iron core.

reluctances and fluxes of saturated core are computed by using the permeabilities and actual BH curve of iron core as shown in Fig. 7. Then, the $k+1$th flux density, B_{ik+1} and magnetic field intensity, H_{ik+1} are calculated by using the reluctances and fluxes.

In the case that the $k+1$th permeabilities are calculated by

$$\mu_{rrc\_ik+1} = \frac{B_{ik+1}}{\mu_0 H_{ik+1}}, \qquad (5)$$

sometimes the permeabilities cannot converge. This is because the permeabilities can oscillate and diverge due to that the updated permeabilities have too high values. The divergence of permeabilities significantly reduces the accuracy of the MEC analysis. Hence, we propose weighted renewal method to update the permeabilities smoothly as follows:

$$\mu_{rrc\_itemp} = \frac{B_{ik+1}}{\mu_0 H_{ik+1}} \qquad (6)$$

$$\mu_{rrc\_ik+1} = \mu_{rrc\_ik+1}\omega_1 + \mu_{rrc\_itemp}\omega_2 \qquad (7)$$

where the weighting values, ω_1 and ω_2 affect the convergence speed and stability. In the case of a large ω_1, since the updated results are largely reflected, the convergence speed is increased. However, for large ω_1, convergence stability of the permeabilities is reduced. On the other hand, in the case of large ω_2, because the conventional permeabilities are mainly considered, the convergence speed is decreased and the convergence stability is increased.

The effect on the convergence speed and stability due to the ω_1 and ω_2 ratio depends on the analysis model. Specifically, the ω_1 and ω_2 ratio, which governs the model convergence, is different with variations in the rotor type, shape and strength of the magnet, and the length of the bridge. In the delta-type IPMSG, as shown in Fig. 2, the nonlinear MEC stably converges when applying an ω_2 value larger than 0.78. Even if ω_2 is 0.9, convergence occurs very quickly within a few seconds. Hence, for the consideration of enhancing the convergence stability according to geometric variations, ω_1 and ω_2 are determined as 0.1 and 0.9, respectively.
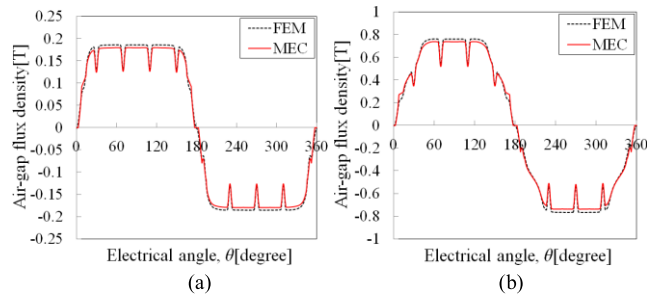

FIGURE 8. Air-gap- flux density of the delta-type IPMSG. (a) 0.5 [T] and (b) 1.3 [T].

Fig. 8 shows the air-gap flux density of the delta-type IPMSG, which is calculated by using the proposed nonlinear MEC method. The shape of the air-gap flux density distribution is changed according to the residual flux density as shown in Fig. 8.

The flux density distributions calculated by the nonlinear MEC and FEM are well matched in Figs. 8(a) and (b), where the residual magnetic flux density, B_r is 0.5 T and 1.3 T, respectively. In other words, the proposed non-linear MEC can precisely calculate the magnitude as well as the shape of the air-gap flux density distribution. The slotting effect is considered by using conformal mapping as discussed in [10], [11].

Fig. 9 and 10 show the flux linkage and back-EMF calculated by the FEM and MEC methods. The equations of flux linkage and back-EMF per phase are as follows:

$$\lambda = N_{ph}B_{ave}A \tag{8}$$

$$E = \frac{d\lambda}{dt} \approx \frac{\Delta\lambda}{\Delta t} = \frac{\Delta\theta}{\Delta t}\frac{\Delta\lambda}{\Delta\theta} = \omega\frac{\Delta\lambda}{\Delta\theta} \tag{9}$$

where N_{ph} is the number of turns per phase, B_{ave} is average air-gap flux density calculated from the air-gap flux density
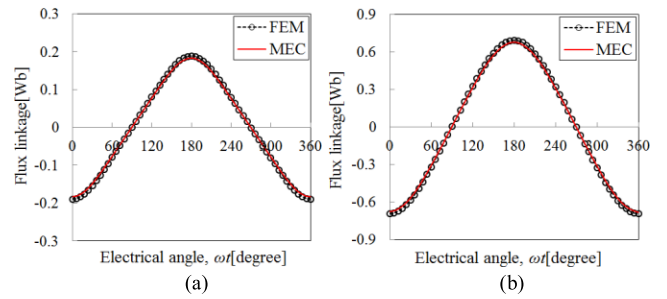

FIGURE 9. Flux linkage of the delta-type IPMSG. (a) 0.5 [T] and (b) 1.3 [T].
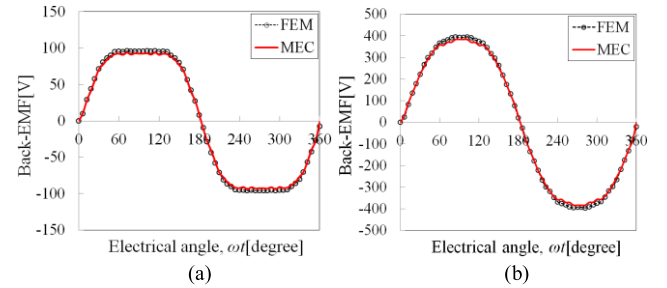

FIGURE 10. Back-EMF of the delta-type IPMSG. (a) 0.5 [T] and (b) 1.3 [T].

TABLE 1. Comparison of the calculated flux linkage by using FEM and MEC.

B_r of PM	Flux linkage$_{max}$ (FEM)	Flux linkage$_{max}$ (MEC)	Difference
0.5 T	0.189 Wb	0.183 Wb	3.06 %
1.3 T	0.694 Wb	0.678 Wb	2.30 %

TABLE 2. Comparison of the calculated back-EMF by using FEM and MEC.

B_r of PM	Back-EMF$_{max}$ (FEM)	Back-EMF$_{max}$ (MEC)	Difference
0.5 T	0.189 Wb	0.183 Wb	3.06 %
1.3 T	0.694 Wb	0.678 Wb	2.30 %

distribution as shown is Fig. 8, A is the area where the magnetic flux passes through the coil, θ is the angular position, and ω is angular velocity of the IPMSG.

The flux linkage and back-EMF calculated by the two different methods also fit well with about a 3 % difference regardless of the residual magnetic flux density, B_r as shown in Fig. 9, Fig. 10, Table 1, and Table 2. Furthermore, Fig. 11 shows that each harmonics of the back-EMF are also well matched.

IV. CONCEPT DESIGN OF DELTA-TYPE IPMSG FOR REEV BY USING NONLINEAR MEC METHOD

A. REQUIREMENT AND CONSTRAINT CONDITION OF DELTA-TYPE IPMSG FOR REEV

Table 3 shows the requirement and constraint condition of delta-type IPMSG for REEV. The rated operating point composed by the rated torque, power, and rotational speed is
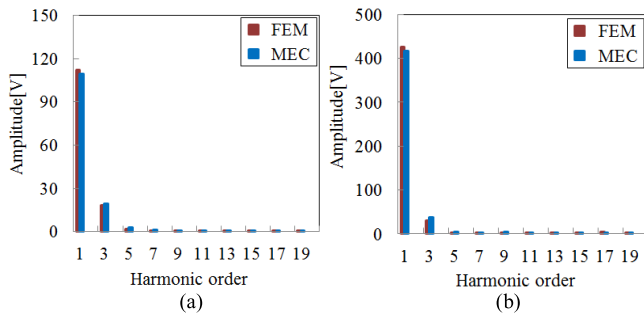
FIGURE 11. Back-EMF harmonics of the delta-type IPMSG. (a) 0.5 [T] and (b) 1.3 [T].

TABLE 3. Specifications of the IPMSG for REEV.

Pole / slot	8 / 36
Rated torque / power	-200 Nm / 60 kW
Rotational speed	3000 rev/min
Stator diameter	220 mm
Airgap	0.9 mm
Battery voltage	210 V_{DC}
Stator and rotor core	35PN230
Permanent magnet	N40UH (B_{rmin} 1.27 T)
Number of coils	33 turns
Parallel circuit	4
Torque ripple	6 %
Efficiency	95 %

FIGURE 12. Mapping results. (a) THD of back-EMF according to α_{p1} and α_{p2}. (b) The fundamental component of the back-EMF according to α_{p1} and α_{p2}.
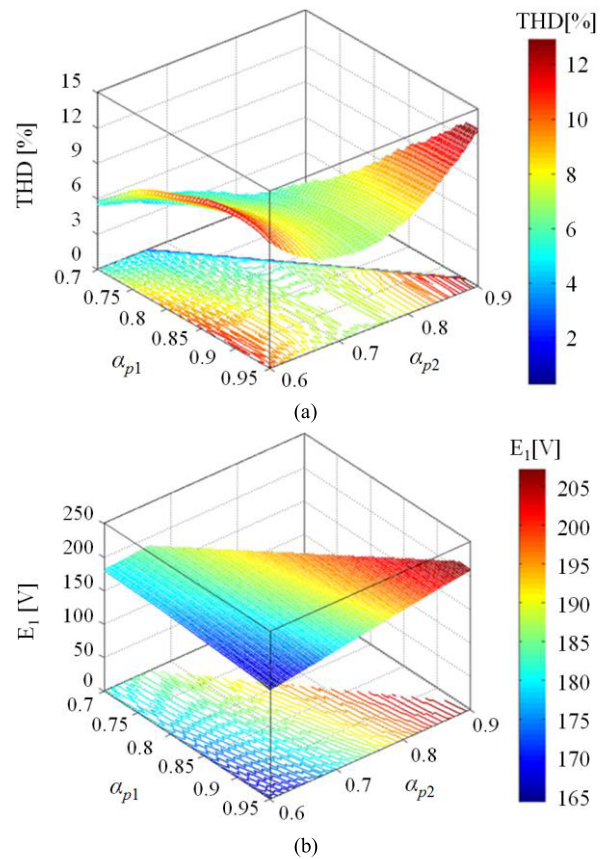
decided in the high-efficiency region of the engine. The charging state of the battery can be maintained even through the REEV drives on the highway based on the world harmonized vehicle cycle, which is used to measure the green-house gas of large vehicles in Europe [12]. In other words, the rated power is determined for maintaining the state of charge of the battery when driving.

The requirement of torque ripple is decided to improve the output power quality, controllability, and riding impression and that of the efficiency is decided to power, size, and cooling method.

B. CONCEPT DESIGN OF IPMSG FOR REEV BY USING THE PROPOSED MEC METHOD

The goal of concept design is to determine the approximate size and shape of the delta-type IPMSG in the initial design stage. Although the FEM can analyze the delta-type IPMSG precisely, it requires a huge computational burden to calculate the model in the initial design stage [6], [7], [9]. Hence, the design efficiency can be significantly improved by using the high speed nonlinear MEC method in the concept design stage for the delta-type IPMSG.

In AC machines like the IPMSG, the fundamental component of the back-EMF generates the effective power and torque. The harmonics cause the torque ripple as well as heating losses [9]. Hence, the power density and quality of the delta-type IPMSG can be improved by the maximization of the fundamental component of the back-EMF and the minimization of the THD of the back-EMF.

To achieve these goals, the mapping results of the fundamental component and the THD of the back-EMF according to the pole arc to pole pitch ratios, α_{p1} and α_{p2} are calculated by using the proposed nonlinear MEC method, as shown in Fig. 12. The design variables, α_{p1} and α_{p2}, largely affect the fundamental component and the THD of the back-EMF. The mapping results of the fundamental component and the THD of the back-EMF represent a different trend. Hence, the combination of α_{p1} and α_{p2} satisfying the design requirements should be selected by considering the importance of the fundamental component and the THD of the back-EMF.

When applying the proposed nonlinear MEC method to the concept design of the delta-type IPMSG, the performances can be effectively analyzed according to changes in various design variables. This is because we can very quickly obtain the mapping results, by using the nonlinear MEC method. In terms of calculation time, it takes several tens of seconds to make the mapping results as shown in Fig. 12 by using the proposed MEC method. However, the FEM requires about several hours to make the mapping results.

Fig. 13 shows the back-EMF results calculated using the proposed nonlinear MEC and measured using the manufactured delta-type IPMSG for the REEV referred in [2].
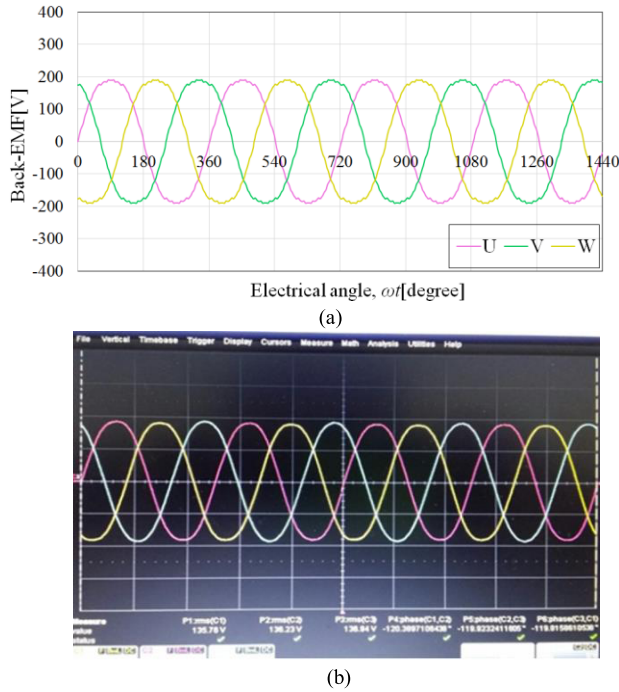
(a)

(b)

FIGURE 13. Back-EMF waveform of (a) the analyzed results by the improved MEC and (b) results measured by the experiment.
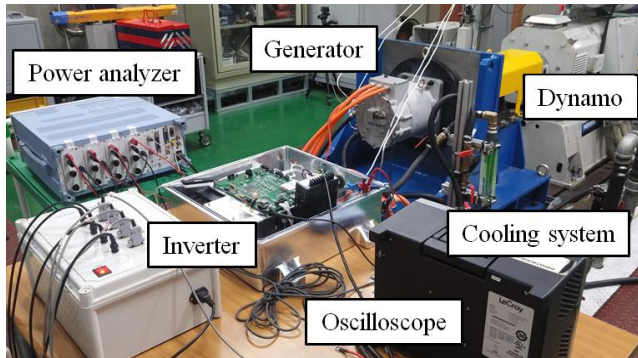

FIGURE 14. Test setup for experiment.

Specifically, the design parameters of the back-EMF result, as shown in Fig. 13 (a), are applied to those of the manufactured IPMSG discussed in [2]. The pole arc to pole pitch ratios, α_{p1} and α_{p2}, of the manufactured model are 0.895 and 0.840, respectively. Since the REEV requires a very high power density, the selected combination of the design variables has a high fundamental component of the back-EMF. The phase RMS values of the back-EMF are well matched, as 138.69 V and 136.31 V, with a 1.72 % error.

By comparing the test results of the manufactured delta-type IPMSG, the accuracy of the nonlinear method is verified. Fig. 14 shows the test setup for the experiment of the manufactured delta-type IPMSG for REEV.

C. SPECIFIC DESIGN FOR REEV BY USING FEM
The main goal of the concept design using the proposed nonlinear MEC is to determine the initial design result

TABLE 4. Comparison analysis and experimental result.

	Analysis (FEM)	Experiment	Difference
Back-EMF	140.79 V	136.31 V	3.29 %
Torque	-203.8 Nm	-202.0 Nm	0.89 %
Torque ripple	4.6 %	4.8 %	4.17 %
Efficiency	97.19 %	95.40 %	1.84 %

considering various design variables. If the initial design result is selected in the concept design stage, load analysis is implemented to satisfy the design requirements such as torque, torque ripple, and efficiency in the specific design stage by using the FEM. The torque, torque ripple, m efficiency results of FEM and experimental are in good agreement as shown in Table 4 and the results satisfy the requirements for REEV.

In summary, through appropriate usage of the proposed MEC in the concept design stage and the FEM in the specific design stage, the efficiency of the design process can be remarkably improved.

V. CONCLUSION
This paper is noteworthy in that the concept design result of the delta-type IPMSG can be obtained quickly and precisely by using the proposed nonlinear MEC method in the initial design stage. Especially, the highly saturated delta-type IPMSG, which has a high power density and a low torque ripple, is accurately analyzed through the nonlinear and iterative analysis with the *BH* curve of the actual steel sheet. Hence, the proposed nonlinear MEC can be widely used for the analysis and design of IPM machines with a high magnetic saturation effect in a variety of applications requiring a high power density and a low torque ripple.

REFERENCES
[1] K. M. Rahman, S. Jurkovic, C. Stancu, J. Morgante, and J. P. Savagian, "Design and performance of electrical propulsion system of extended range electric vehicle (EREV) chevrolet volt," *IEEE Trans. Ind. Appl.*, vol. 51, no. 3, pp. 2479–2488, May/Jun. 2015.

[2] D.-K. Lim, S.-Y. Jung, K.-P. Yi, and H.-K. Jung, "A novel sequential-stage optimization strategy for an interior permanent magnet synchronous generator design," *IEEE Trans. Ind. Electron.*, vol. 65, no. 2, pp. 1781–1790, Feb. 2018.

[3] J. W. Jiang, B. Bilgin, A. Sathyan, H. Dadkhah, and A. Emadi, "Analysis of unbalanced magnetic pull in eccentric interior permanent magnet machines with series and parallel windings," *IET Electr. Power Appl.*, vol. 10, no. 6, pp. 526–538, Jul. 2016.

[4] S. Lee, K. Kim, S. Cho, J. Jang, T. Lee, and J. Hong, "Optimal design of interior permanent magnet synchronous motor considering the manufacturing tolerances using Taguchi robust design," *IET Electr. Power Appl.*, vol. 8, no. 1, pp. 23–28, Jan. 2014.

[5] M. Barcaro, A. Faggion, N. Bianchi, and S. Bolognani, "Sensorless rotor position detection capability of a dual three-phase fractional-slot IPM machine," *IEEE Trans. Ind. Appl.*, vol. 48, no. 6, pp. 2068–2078, Nov./Dec. 2012.

[6] R. Lin, S. D. Sudhoff, and C. Krousgrill, "Analytical method to compute bridge stresses in V-shape IPMs," *IET Electr. Power Appl.*, vol. 12, no. 7, pp. 938–945, Aug. 2018.

[7] L. Zhu, S. Z. Jiang, Z. Q. Zhu, and C. C. Chan, "Analytical modeling of open-circuit air-gap field distributions in multisegment and multilayer interior permanent-magnet machines," *IEEE Trans. Magn.*, vol. 45, no. 8, pp. 3121–3130, Aug. 2009.

[8] L. Chong and M. F. Rahman, "Saliency ratio derivation and optimisation for an interior permanent magnet machine with concentrated windings using finite-element analysis," *IET Electr. Power Appl.*, vol. 4, no. 4, pp. 249–258, Apr. 2010.

[9] D.-K. Lim, K.-P. Yi, D.-K. Woo, H.-K. Yeo, J.-S. Ro, C.-G. Lee, and H.-K. Jung, "Analysis and design of a Multi-Layered and multi-segmented interior permanent magnet motor by using an analytic method," *IEEE Trans. Magn.*, vol. 50, no. 6, Jun. 2014, Art. no. 8201308.

[10] H. Mirahki, M. Moallem, M. Ebrahimi, and B. Fahimi, "Combined ON/OFF and conformal mapping method for magnet shape optimisation of SPMSM," *IET Electr. Power Appl.*, vol. 12, no. 9, pp. 1365–1370, Nov. 2018.

[11] E. Costamagna, P. D. Barba, and A. Savini, "Conformal mapping of doubly connected domains: An application to the modelling of an electrostatic micromotor," *IET Electr. Power Appl.*, vol. 3, no. 5, pp. 334–342, Sep. 2009.

[12] Q. Yuan, "Real world duty cycle development method for non-road mobile machinery (NRMM)," *SAE Int. J. Commer. Veh.*, vol. 9, no. 2, pp. 306–312, Sep. 2016.

DONG-KUK LIM received the B.S. degree in electrical engineering from Dongguk University, Seoul, South Korea, in 2010, and the Ph.D. degree in electrical engineering from Seoul National University, Seoul, in 2017, through the combined Master's and Doctorate Program.

In 2017, he was a Senior Research Engineer with the Electrical Power Engineering Team, Hyundai Mobis Company, South Korea. He is currently an Assistant Professor with the School of Electrical Engineering, University of Ulsan, South Korea. His research interest includes analysis and optimal design of electrical machines.

JONG-SUK RO received the B.S. degree in mechanical engineering from Hanyang University, Seoul, South Korea, in 2001, and the Ph.D. degree in electrical engineering from Seoul National University (SNU), Seoul, in 2008.

He was a Senior Engineer and conducted research at the R&D Center of Samsung Electronics, from 2008 to 2012. From 2012 to 2013, he was a Postdoctoral Fellow with the Brain Korea 21 Information Technology, SNU. He was a Researcher and conducted research at the Electrical Energy Conversion System Research Division, Korea Electrical Engineering and Science Research Institute, in 2013. From 2013 to 2016, he was a BK Assistant Professor with the Brain Korea 21 Plus, SNU. In 2014, he was with the University of BATH, Bath, U.K. He is currently an Associate Professor with the School of Electrical and Electronics Engineering, Chung-Ang University, Seoul. His research interest includes the analysis and optimal design of next-generation electrical machines using smart materials, such as electromagnet, piezoelectric, and magnetic shape memory alloy.

• • •